AUTOMATED CALCULATION OF THE INTERNAL STRUCTURE AND THE NATURAL FREQUENCIES OF HELICOPTER ROTOR BLADES WITH REGARD TO AUTOMATED ROTOR BLADE OPTIMIZATION

Franziska Becker, Steffen Kalow,
German Aerospace Center (DLR) / Institute of Lightweight Systems, Braunschweig, Germany
Rainer Bartels,
German Aerospace Center (DLR) / Institute of Flight Systems, Braunschweig, Germany

Abstract

With regard to an automated multidisciplinary optimization process an automated modeling and calculation of the structural properties of helicopter rotor blades was aspired. For this purpose, a program for structural rotor blade modelling based on rotor blade cross-sections was developed. This process is implemented as three successive steps. First, the CAD cross-section geometry is generated on the basis of a geometry template. Based on this, a structural model is generated and the structural properties are calculated with DLR inhouse tool SaMaRA. Finally, the natural frequencies are calculated using a beam model according to Houbolt & Brooks. To investigate the internal structure of a given outer blade geometry, the sensitivity of structural parameter variations was carried out. For this purpose, a uniform shaped rotor blade based on a selected cross-sectional topology in the aerodynamic blade region was considered. The performed parameter study considers the effects of different parameter intervals on the structural properties and the resulting natural frequencies.

1. NOTATION

Symbols

c	Chord,m; stiffness, Nm^2
EA	Tension stiffness, N
EI_f	Flap stiffness, Nm^2
EI_l	Lead-lag stiffness, Nm^2
GI_t	Torsional stiffness, Nm^2
m	Mass, kg
Ω, Ω_{ref}	Rotor speed of rotation, rad/s
ω_0	Natural frequency, Hz

Acronyms:

ANSYS WB	ANSYS Workbench
CAD	Computer Aided Design
CATIA	Computer Aided Three-Dimensional Interactive Application
CG	Center of gravity, m
CPACS	Common Parametric Aircraft Configuration Schema
DTCTE	Distance Torsion Cap Trailing Edge
DSCMR	Distance Spar Center Main Radius
DSTE	Distance Spar Trailing Edge
F_i	Flap natural frequency
FTK	Advanced Swashplate Concepts
RBG	RotorBladeGenerator
L_i	Lead-Lag natural frequency
SaMaRA	Structural Modeling and Rotor Analysis
SC	Shear center, m
SFA	Spar flange angle, °
SFT	Spar Flange Thickness
S4 FEM	S4 Preprocessor
T_i	Torsional natural frequency
TC	Tension center, m
TCT	Torsion Cap Thickness
VicToria	Virtual Aircraft Technology Integration Platform
XML	Extensible Markup Language

Copyright Statement

The authors confirm that they, and/or their company or organization, hold copyright on all of the original material included in this paper. The authors also confirm that they have obtained permission, from the copyright holder of any third-party material included in this paper, to publish it as part of their paper. The authors confirm that they give permission, or have obtained permission from the copyright holder of this paper, for the publication and distribution of this paper as part of the ERF proceedings or as individual offprints from the proceedings and for inclusion in a freely accessible web-based repository.

2. INTRODUCTION

Nowadays, modern helicopter rotor blades are optimized in the first step with regard to their aerodynamic shape, considering the complex requirements resulting from the different flight conditions. The dynamic properties of a helicopter rotor blade, on the other hand, are determined by the stiffness and mass distributions that result from the structural design. Based on the outer shape of the aerodynamic skin, which limits the design space of the inner geometry elements, cross-sectional profiles can also vary in their airfoil sizes in the spanwise direction of the rotor blade. Variations in the material selection and dimensioning of the inner geometry elements, such as the rotor blade skin and spar, and the resulting structural properties, influence the natural frequencies of a rotor blade and thus the rotor in its vibration behavior. With regard to an automated multidisciplinary optimization process, there are already approaches for adapting the properties of the rotor blade structure model based on scaling laws, as described in Bailly et al. Ref. 1 and Stanger et al. Ref. 2. Another approach by Desvigne et al. Ref. 3 relates to a structural adjustment based on similar reference rotor blades, whose natural frequencies are known in advance. The accuracy of the calculation results is largely determined by the quality of the reference model and its transferability to the model to be optimized. However, calculation methods of higher complexity, which include all design variables relevant for the inner rotor blade design, are computationally and thus cost intensive. Therefore, an automated modeling for helicopter rotor blades is aspire to. Another approach by B. Haehnel et al. Ref. 4 presents an inverse process, where a cross-section design is determined based on already known structural properties of a reference rotor blade.

Focusing on the structural characterization of rotor blades, a design chain with integrated structural design was developed in Kalow et al. Ref 5. The structural rotor blade modeling and calculation follows the common approach, Ref. 6, of discretization, in terms of rotor blade cross-sections, in the spanwise direction. An example of this is presented by Kalow in Ref. 5 within the described design chain, where the tool for the analysis of cross sections SaMaRA is applied. The construction of a structural model with varying cross-sectional dimensions and complex internal structural design is very time consuming in manual implementation and thus associated with high costs. Therefore, in the course of the DLR-project VicToria (Virtual Aircraft Technology Integration Platform) an automated generation of structural models and calculation of structural properties of rotor blade cross-section geometries with high accuracy was developed by Bram van de Kamp Ref. 7. In the DLR project Urban Rescue this approach was followed up and extended to calculate the natural frequencies.

To determine the sensitivity of parameter variations of the anisotropic internal structural elements to the structural properties, such as stiffness, inertia and rotor blade axis positions, a parameter study and frequency analysis was conducted.

3. ROTOR BLADE DESIGN PROCESS

To determine the structural properties and the eigenfrequencies of a rotor blade, the DLR inhouse tool RotorBladeGenerator (RBG) was developed and used. For this design process, several subroutines were written and combined into a Python frame work. This controls the automated process for reading in the relevant process parameters and makes them available to the respective program part. The calculation of the structural properties of a cross-section as well as the subsequent natural frequency analysis is performed in five steps as shown in Figure 1. First the Input XML-file, based on the CPACS schema and containing all information of all cross-sections along the rotor blade in radial direction, was created. This model information includes cross-section position and orientation, point coordinates, material properties and composite lay ups, PowerCopy (template for CAD software CATIA), material and mesh assignment to geometry bodies as well as parameterization of each defined cross-section. With respect to the generation of the CAD cross-section geometry, a predefined cross-section design containing the arrangement and dimensioning of the internal structural elements, as shown in Figure 2, is provided to the process in the form of an CATIA-CAD input file. Based on the airfoil point coordinates and the topology template the internal CATIA-CAD-layout is generated. In this process, the given template is adapted to the current cross-section. Using the previously created CAD geometry, the structural model is generated with ANSYS Workbench (WB). The structural model generated in this way contains all the material properties assigned to the various geometry elements.

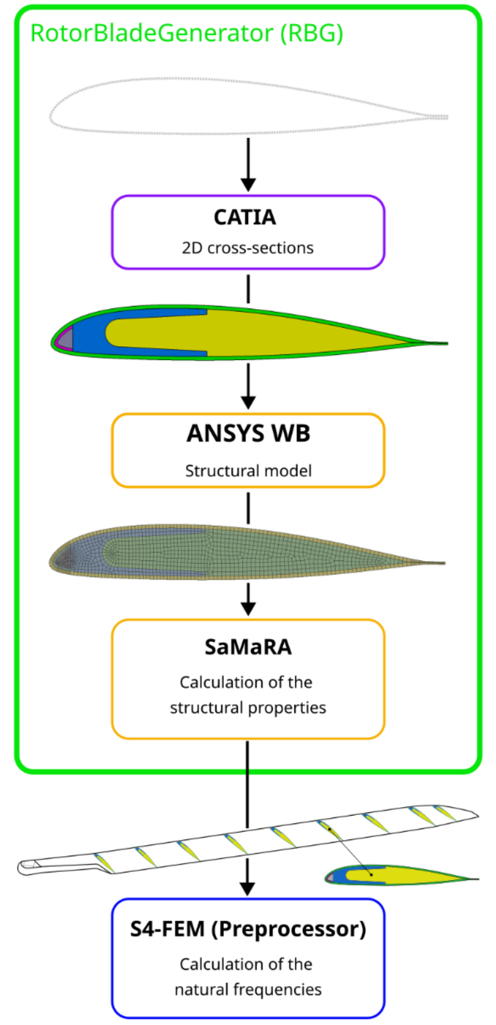

Figure 1: Structural Design Process Ref. 3

This includes for example skin or spar, as well as their layer structure, fiber orientation, layer thickness and number of layers. For calculating the structural properties, the meshed structural model is provided to the DLR inhouse tool SaMaRA (Structural Modeling and Rotor Analysis). Inside SaMaRA, the previously generated structural model is adapted to the different analyses for determining structural properties such as bending stiffnesses, inertias and axis positions. The calculation meshes as well as the boundary conditions and load case are adapted to get the respective structural property. After determining the structural properties for each cross-section, the natural frequencies are calculated using DLR's in-house tool S4-FEM. S4-FEM uses an FEM beam model according to Houbolt & Brooks Refs. 9, 10.

4. SENSITIVITY ANALYSIS

The dynamics of a rotor blade are largely determined by its internal structural design and the rotor speed. Stiffness and mass are the relevant factors for the vibration behavior of a rotor blade. Furthermore, the center of gravity, shear, and tension center are influencing variables and are particularly important for dynamic stability. In the parameter study of Becker et. al Ref. 8, the effects on the stiffness and mass due to variation of different geometric parameters were investigated.

To carry out the sensitivity analysis, one parameter is varied within a specified parameter interval, with all other parameters being kept constant. Manufacturing restrictions, such as the number of layers of the rotor blade skin, are considered in the form of discrete increments in the parameter interval. All other parameter increments are unrestricted, but are preferably selected in equidistant steps. The extremes of the parameter intervals do not necessarily represent realistic parameter constellations in terms of a planned Optimization. Rather, the influence of individual parameters on the stiffness of the cross-section is to be examined, with the variation of the parameter of one geometric element often having an influence on the dimensioning of another geometric element. For this purpose, the structural properties of each individual parameter constellation are calculated within the interval selected for each parameter using the SaMaRA tool. The determined stiffness, mass and axis position data are then evaluated in the form of diagrams.

4.1 Rotor blade cross-section model

In order to get a realistic impression of the structural properties resulting from parameter variations a representative cross-section of the aerodynamic region of the FTK-rotor blade Ref. 5, 11 was chosen to carry out the sensitivity analysis. The FTK rotor is a 1:2.75 Mach scaled wind tunnel model of EC145 rotor. The rotor blade cross-section shown in Figure 2 is defined by seven parameters. The structural design of the FTK-rotor blade consists of the rotor blade skin, a torsion cap, a nose weight, a C-spar and the foam that fills the cavity behind the spar. The rotor blade skin primarily serves to absorb the torsional loads and is made of carbon fabric. A step size in the parameter interval includes one fabric layer, which consists of carbon fibers with $\pm 45°$ fiber orientation. Due to the manufacturing of the FTK-rotor blade in a split mold a torsion cap is implemented.

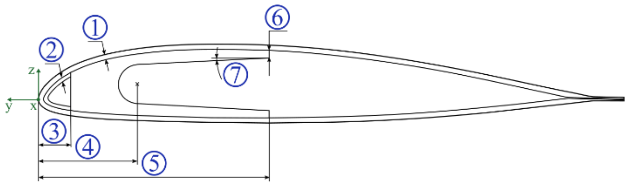

Figure 2: Parameterization of 2D cross-section

This firmly connects the upper and lower rotor blade halves in the area of the leading-edge Ref. 11. In addition, this serves to close the torsion box and limits the nose weight in its size. At this point, it should be mentioned that the parameter “Torsion Cap Thickness” (TCT) parameter is not a useful design parameter for optimization. By varying TCT, the effect of the nose weight on the natural frequencies should be represented. The nose weight (tungsten-resin-mixture) is used for adjustment of the center of gravity in the near of the quarter chord ($c/4$) location. In addition, a c-formed spar which usually consists of composite material with unidirectional fiber orientation in radial rotor blade direction is implemented. This serves to transfer the resulting bending loads as well as to absorb the centrifugal load. The foam filling the remaining cavity serves to maintain the shape retention of the rotor blade profile. The parameter - material and fiber orientation - remain constant for this investigation. The minimal skin and torsion cap thickness is set to one composite layer.

4.2 Results

Since the values of the respective stiffnesses and mass differ by up to two orders of magnitude, they are presented normalized based on its maximum. For example, tension stiffness ($EA \approx 10^7 N$) is five orders of magnitude higher than the flap and torsional stiffness ($EI_f, GI_t \approx 10^2\ Nm^2$) and four orders of magnitude higher than the lead-lag bending stiffness ($EI_l \approx 10^3 Nm^2$). All stiffness and mass values of the investigated parameter intervals are shown in Figure 9 and Figure 10 (left sided diagrams). The parameter increments visualized on the abscissa are normalized to its parameter interval. The axis movements of the parameter intervals are shown in percent of the chord and thickness length in Figure 9 and Figure 10 (right sided diagrams).

4.2.1 Skin Thickness

The rotor blade skin made of carbon fabric and $\pm 45°$ fiber orientation serves to absorb load-induced torsional moments. Accordingly, the torsional stiffness is increased the most by introducing additional layers. Simultaneous to changing the torsional stiffness, the position of the shear center is also varied in the interval in a wide range. The shear center has to be placed as close as possible to $c/4$ due to stability restrictions. Increasing the thickness of the skin based on the starting configuration is a possibility to increase torsional as well as lead-lag stiffness and the movement of the shear center towards $c/4$. Because of the coupling in between the change of one parameter and the effect on all inner geometry components and therefore the structural properties resulting from that, the center of gravity (CG) is influenced stronger than the shear center (SC) at the same time. For example, because of the increase of the skin thickness the nose weight cross-section area decreases significantly. This moves the CG further away from $c/4$. Therefore, another parameter must be found that compensates for the offset from $c/4$ and CG. As can be seen in Figure 3 the increase of the skin thickness results in a decrease of the nose weight cross-sectional area.

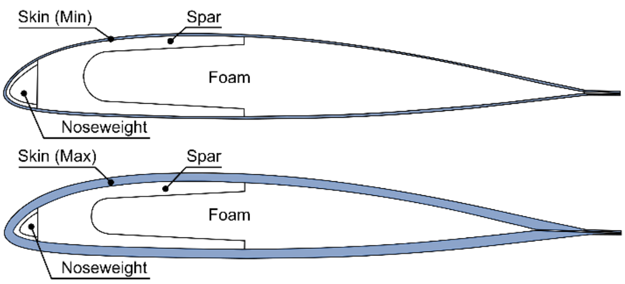

Figure 3: Extrema skin thickness

In addition to these effects, which are essential for the thickness of the skin, further side effects result from the geometry couplings. For example, the lead-lag stiffness is increased by additional fibers implemented with a large distance to $c/4$ in the trailing edge region. This affects also the position of the tension center (TC) and will increase its distance to $c/4$. An offset of the TC from $c/4$ leads to a bending of the rotor blade in lead-lag direction due to the centrifugal load, which can be undesirable. The tensile stiffness is increased rather slightly over the parameter interval compared to torsional and lead-lag stiffness. Here, the reduction of the spar area by approx. 8% and the increase of the skin area by 75% counteract each other at the maximum limit. The 0° oriented glass fibers in the outer area cross-section of the spar are replaced by $\pm 45°$ oriented carbon fibers and additionally introduced in the rear area of the airfoil cross-section.

4.2.2 Torsion Cap Thickness

The cap of the FTK-rotor blade is made of $\pm 45°$ carbon fabric. It is used to close the torsion box when manufacturing in split molds. In addition, the torsion cap constrains the nose weight (tungsten-resin-mixture) dimensions. The parameter extrema are shown in Figure 4.

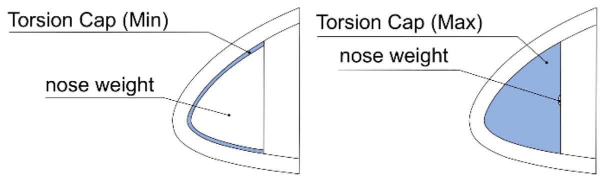

Figure 4: Extrema torsion cap thickness

The parameter TCT is used to show the influence of the nose weight or the carbon fibers in the front area of the rotor blade cross-section. Although the parameter is not suitable as a design variable in the sense of an optimization, since the thickness of the torsion cap is predefined anyway, the influence of the nose weight on the natural frequencies can be separately determined by varying TCT. As can be seen in the diagram, Figure 9 and Figure 10, all values concerning stiffness are hardly varied with variation in TCT. Only the change in mass is visible. Accordingly, only the CG of the axis positions diagram shows a variation over parameter interval. In the context of an optimization, this parameter can be neglected, since the size of the nose weight is regulated by the distance to the trailing edge of the torsion cap.

4.2.3 Distance Torsion Cap Trailing Edge

The parameter "Distance Torsion Cap Trailing Edge" (DTCTE) on the one hand increases the size of the nose weight and on the other hand simultaneously reduces the spar cross-section area at the leading-edge region. This is shown in Figure 5. Due to the increase of the nose weight the CG is varied in a wide range. The increase allows the CG to be shifted towards $c/4$, as can be seen in the axis positions diagram Figure 9. The distance between CG and $c/4$ has an important influence on the static stability of a rotor blade. A greater offset of CG behind $c/4$ leads to an increase in the blade angle of attack, which in turn can lead to large elastic torsion angles due to small disturbances in flight, Ref. 12. Therefore, the distance between CG and $c/4$ should be kept as small as possible. Regarding an optimized parameter constellation for example, a thicker skin and a reduced nose weight could be compensated for by this parameter. With regard to stability, the smallest possible offset between SC and CG helps to avoid the flutter phenomenon.

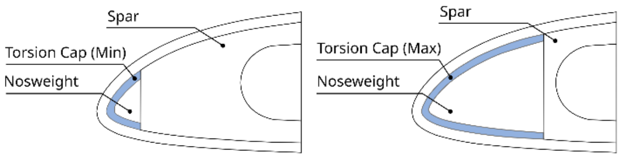

Figure 5: Extrema distance torsion cap leading edge

The loss of spar cross-section area results in a decrease in tensile and lead-lag stiffness and an increase in the offset between $c/4$ and the tension center (TC). This may have to be compensated for by another parameter.

4.2.4 Spar Flange Thickness and Angle

The parameters "Spar Flange Thickness" (SFT) and "Spar Flange Angle" (SFA) show similar characteristics in its mode of action and therefore result in corresponding stiffness properties, with the increase in stiffness for the parameter SFT being somewhat greater. Therefore, the parameter SFT is considered in more detail and visualized in Figure 6.

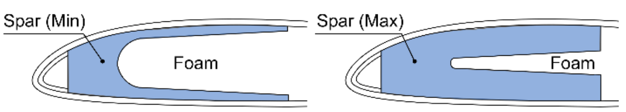

Figure 6: Extrema spar flange thickness

Due to the dependence on the Young's modulus of the spar material as well as shape and sizing of the cross-sectional area of the spar, the tension stiffness (EA) is most strongly influenced by this parameter. If the spar flanges become very narrow, the flap stiffness (EI_f) is reduced compared to the starting configuration. Furthermore, the spar cross-section area is increased up to 54% inwards. The cross-sectional centers, on the other hand, are only slightly influenced by this parameter. The axis positions are shown Figure 9 in. The material placement and thus both mass and stiffness changes take place at a small distance from $c/4$. As the distance to $c/4$ decreases, the influence on the lag and in particular flap stiffness also decreases. In general, the flap stiffness and the tension stiffness can be varied by this parameter with only slightly effect on the axis positions.

4.2.5 Distance Spar Center Main Radius

The parameter "Distance Spar Center Main Radius" (DSCMR) varies the amount of fiber material inside the C-spar. As shown in the Figure 7, in the parameter minimum there is hardly any web in between the spar flanges, while in the maximum the spar is almost completely filled and resembles a filled D-shape.

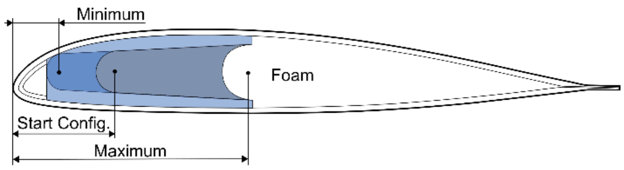

Figure 7: Extrema spar center main radius

The difference of spar cross-section area in between minimum and maximum is 64%. Accordingly, the tension stiffness, as shown in Figure 10, is varied the most. The influence of the unidirectional glass fiber material in the cross-section leading-edge region on the lead-lag stiffness becomes visible in the interval between the parameter minimum and the starting configuration. Here the lead-lag stiffness is increased the most in contrast to the rest of the interval. Similar to the parameter SFT, the flap stiffness increases with the increase in fiber material in the center of the spar. For the axis positions, shown in Figure 10, the positions of SC and CG approach $c/4$ in the area between the starting configuration and the parameter maximum. In contrast to the skin thickness parameter, SC is more strongly influenced than CG in this parameter (DSCMR). Since the mass in the cross-section is also significantly increased by filling the spar, the use of a D-spar in place of the C-spar could be considered.

4.2.6 Distance Spar Trailing Edge

Following the curved outer contour of the rotor blade cross-section, the spar flanges in the area of the trailing edge are brought closer to the inside when the parameter tends towards its maximum. Parameter minimum and maximum are shown in Figure 8. Similar to the parameter "Distance Spar Trailing Edge" (DSTE), the spar cross-section area and thus also the tension stiffness are greatly increased up to 84% in the parameter interval. Furthermore, in the diagram Figure 10, the importance of the spar flanges for the flap stiffness can be seen.

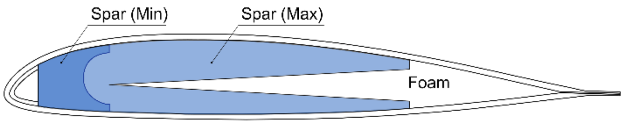

Figure 8: Extrema distance spar trailing edge

Following the flap stiffness curve in the diagram the center of the interval shows the strongest rise in flap stiffness values. Furthermore, the increase in the stiffness values falls off somewhat towards both parameter minimum and maximum. Contrary to the flap stiffness, a clear and strong increase is only visible for the lead-lag stiffness in between the starting configuration and the maximum in the diagram. The further towards the maximum the spar flanges are lengthened from the starting configuration, the more significantly the lead-lag stiffness increases. Since the spar area increases significantly over the parameter interval, the mass also increases significantly, which, as expected, also has a strong effect on CG and TC with regard to axis positioning also shown in Figure 10. SC is also strongly influenced by the strong increase in additional introduced unidirectional glass fibers. For a differentiated assessment of the influence of the spar flanges separately from the strong increase in spar area inside the spar, the use of a spar geometry without flange angle should be considered.

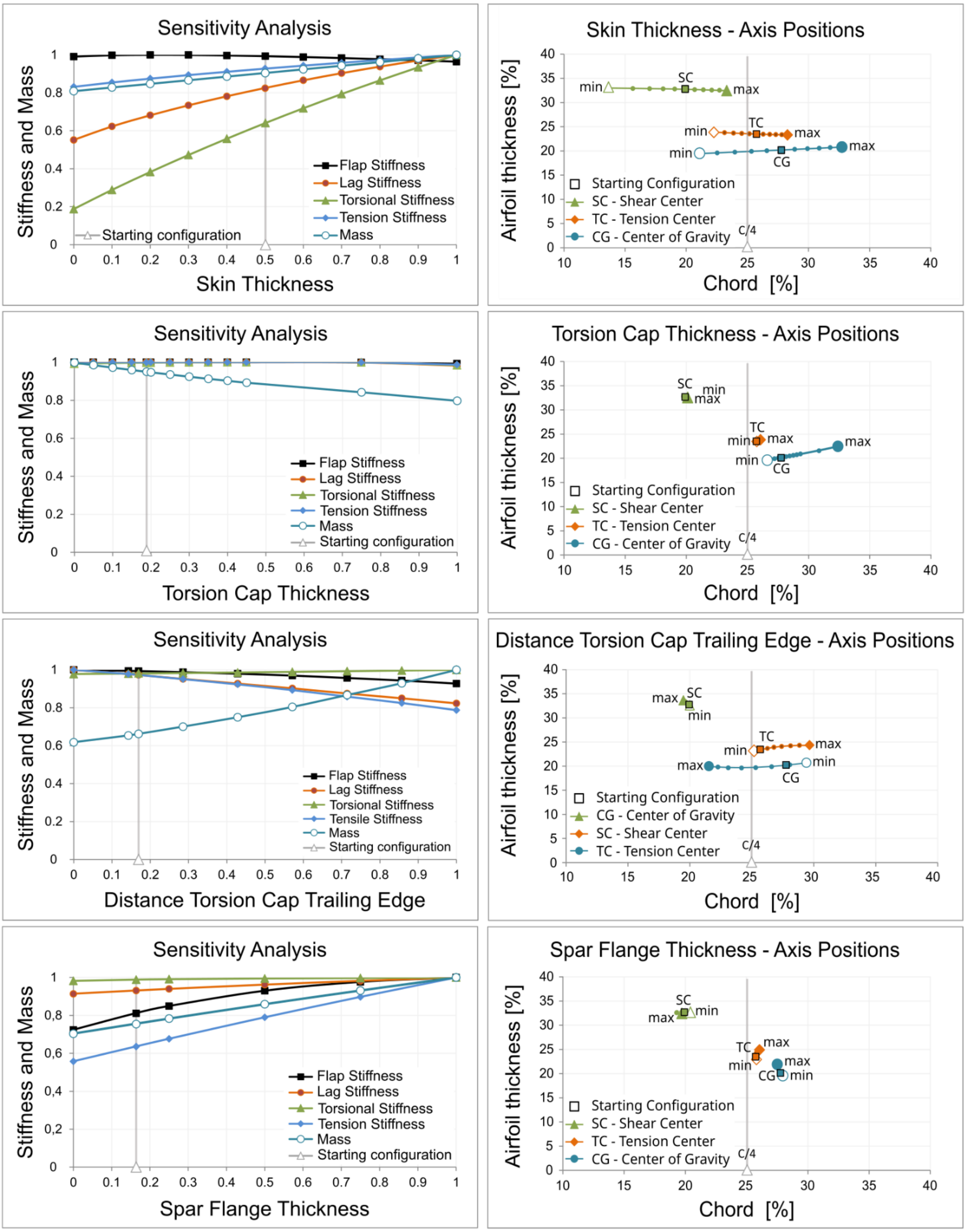

Figure 9: Sensitivity results (stiffness, mass and axis positions)

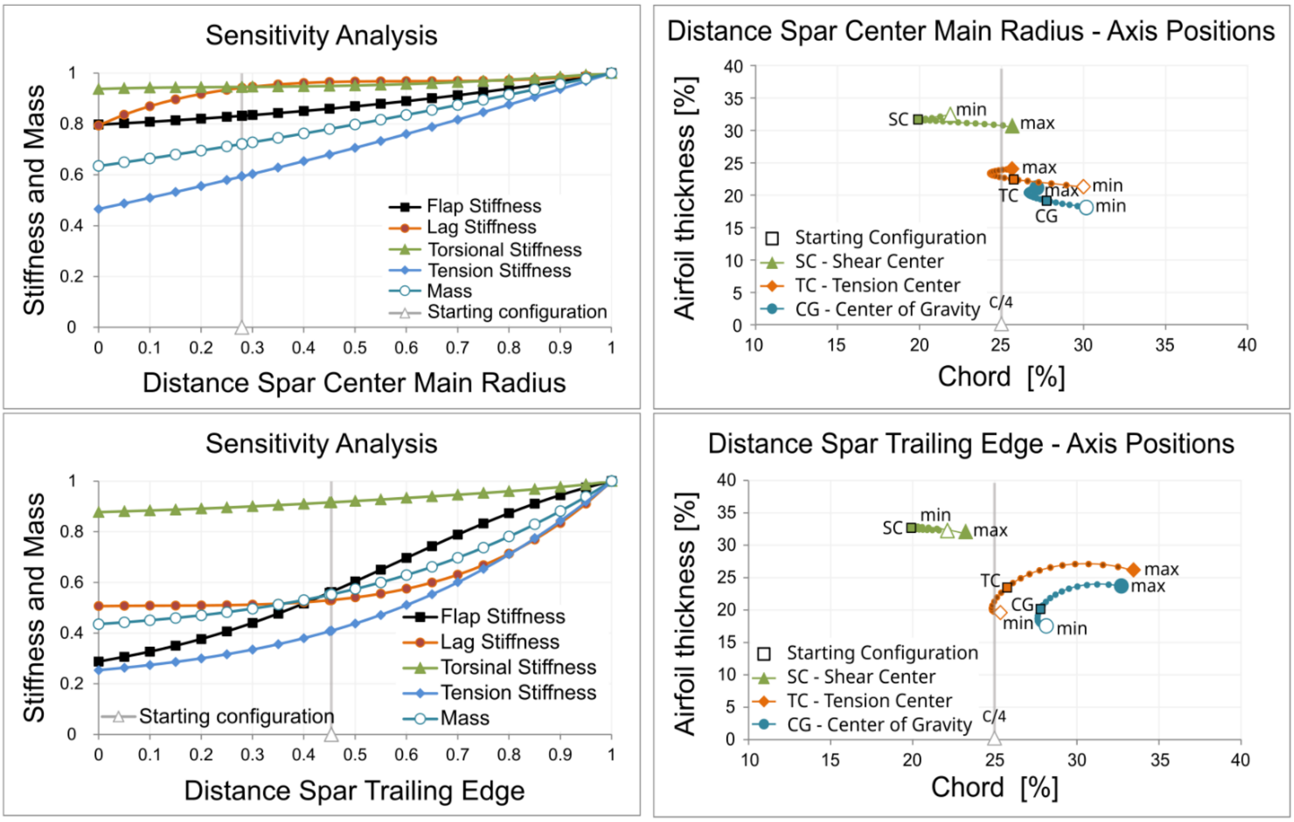

Figure 10: Sensitivity results (stiffness, mass and axis positions)

5 FREQUENCY ANALYSIS

With the help of the natural frequency analysis, an initial estimate of the dynamics of a rotor blade is made after the structural design. This is an important step in identifying critical natural frequency placements that can result in dynamically unstable vibration behavior. For the frequency analysis an ensemble of all cross-sectional properties resulting from the parameterized cross-sectional topologies are examined. In addition to the stiffness, the mass is also considered as an important influencing variable on the vibration behavior. The natural frequency analysis is carried out with the help of the DLR in-house preprocessor Ref. 5 of the S4 program. Since the parameters SFA and SFT are very similar in their mode of action, the natural frequency analysis is limited to the parameter SFT. Also, only the extremes of parameter intervals were examined. Compared to the sensitivity analysis, the influence of the mass in included in the investigation in order to obtain the most realistic possible representation of the mode of action of the individual parameters.

5.1 Rotor blade beam model

For the natural frequency analysis, the cross-sectional properties previously obtained from the sensitivity analysis are combined into a beam model. The chord length as well as the used airfoil and cross-section topology is kept constant in spanwise direction. This results in a uniform rectangular blade shape.

5.2 Results

The results obtained from parameter variation are shown in the rotor frequency diagrams of the respective parameter evaluation. The rotor frequency diagram shows the lower natural frequencies as a function of the normalized rotational speed Ω/Ω_{ref}. It should be mentioned that in areas where curves approach each other, frequency coupling occurs. The course of the curve follows that of the coupled natural frequency. For better orientation the natural frequencies shown in the diagrams include flap frequencies (F1-F5), lead-lag frequencies (L1, L2) as well as the torsional frequency (T1). To get a better overview of the curve movement for the parameter minimum and maximum, these are highlighted with arrows following the orientation of the curve movement. The focus of the examination of the parameter extremes is on the characteristics of the curve movements.

5.2.1 Frequency analysis – Skin Thickness

As shown in the frequency diagram Figure 11, the largest deviation from the initial configuration can be observed for the torsional natural frequency (T1), as expected. Although the start configuration is centered in the parameter interval, see Figure 9, resulting torsional frequencies placed asymmetrically to the start configuration in minimum and maximum.

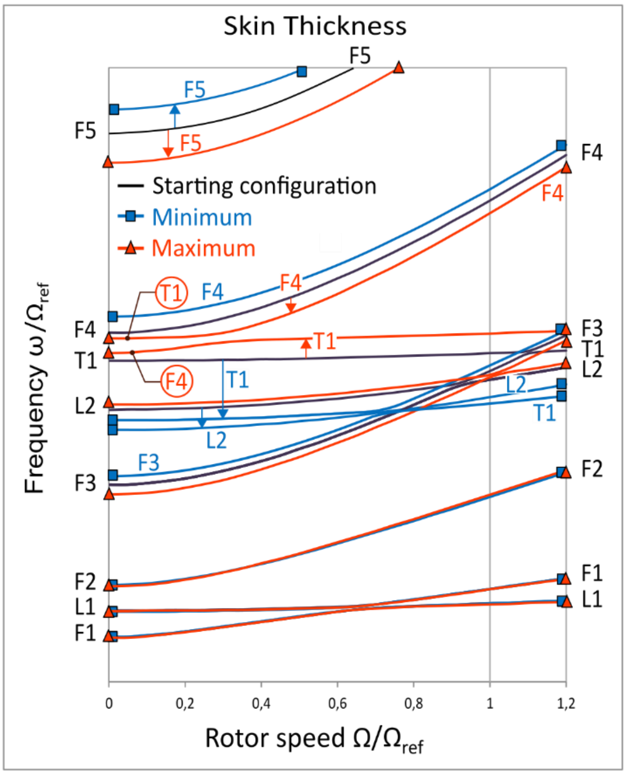

Figure 11: Extrema Frequency analysis – Skin Thickness

On the one hand, the effectiveness of the implemented carbon fibers depends on the lever arm, which results from the distance between the cross-section $c/4$ and the material positioning within the cross-section. On the other hand, with each additional $\pm 45°$ fabric layer applied towards the interior of the airfoil cross-section, less fiber material is introduced than at the outer edge of the airfoil cross-section. Therefore, reducing the skin thickness will decrease the torsional natural frequency more than adding more skin layers will increase it. A similar effect can be observed for the lead-lag natural frequency (L2). The next greatest frequency movement according to the starting configuration can be observed for the upper flap frequencies (F3-F5). While the parameter maximum leads to an increase in the torsional (T1) and lead-lag (L2) eigenfrequency the parameter minimum leads to a decrease. In case of the flap eigenfrequency exactly the opposite effect can be observed, as can be seen in Figure 9. Furthermore, the deviation of the flap frequency minimum and maximum seems to be symmetric about the starting configuration. In addition to the respective stiffnesses, the natural frequencies are also significantly influenced by the resulting change in mass as a result of the parameter variation. The relationship between the mass (m) and the stiffness (c) as shown in formula Eq. (1) applies to the natural frequency (ω_0).

$$\omega_0 = \sqrt{\frac{c}{m}} \tag{1}$$

Over the parameter interval, the mass was increased up to 20% towards the maximum. Further, the variation of the mass over the parameter interval with respect to the starting configuration is similar to the movement of the flap frequencies (F3-F5). Accordingly, the natural flap frequencies are significantly influenced by the mass variation. Finally, the parameter skin thickness has a negligibly small influence on the lower natural frequencies (F1, L1, F2). These show a significantly lower sensitivity to structural parameter changes in the aerodynamic area of the rotor blade compared to the rotor blade root. In addition, the mass variation in general is rather small compared to the mass variation resulting from the other parameters considered.

5.2.2 Frequency analysis – Torsion Cap Thickness

As described in 4.2.2, the size of the nose weight and thus the position of CG is influenced by the parameter TCT. Through the parameter TCT, the influence of the nose weight on the natural frequencies can be observed. Since the variation of the stiffnesses is negligible small for this parameter, the influence of the mass on the natural frequencies can be extracted. It must be noted that the maximum of TCT results in a minimum for the noseweight. In the overview of the natural frequencies in Figure 12, it can be seen that the trend for minima and maxima is the same for all natural frequencies, contrary to the observation from Figure 11.

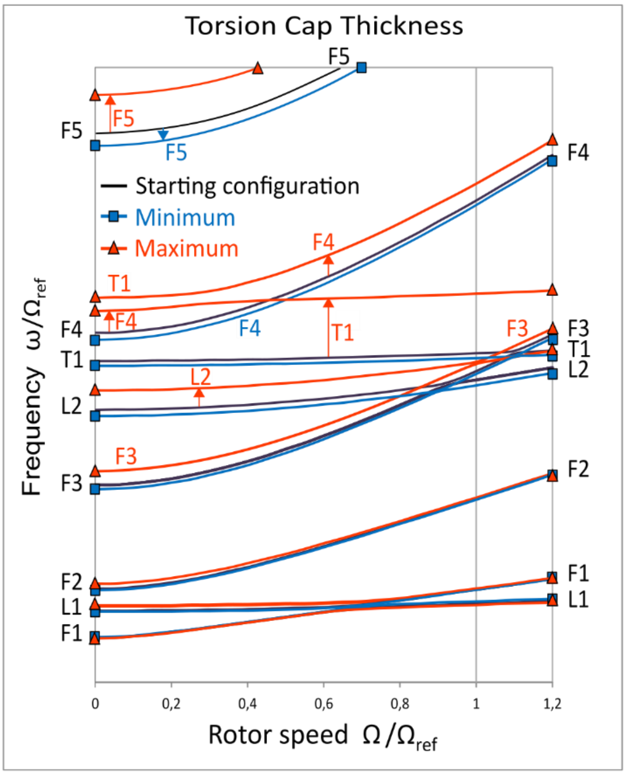

Figure 12: Frequency analysis – Torsion Cap Thickness

Compared to the skin thickness parameter, the cross-sectional mass is decreased over the parameter interval of TCT, but with similar magnitude of 20%. Therefore, the flap frequencies for minimum and maximum have different trends when comparing the change in skin thickness to the change in thickness of the torsion cap. Furthermore, the parameter minimum has a much smaller distance from the starting configuration as the maximum. The maximum offset can again be observed for the torsional natural frequency. In the parameter maximum the nose weight is almost nonexistent, as visualized in Figure 4. The CG has also a big distance from $c/4$ in the parameter maximum as discussed in 4.2.2. With approximately constant stiffness values and decreasing mass over the parameter interval, an increase in the natural frequency for the torsional natural frequency and the lead-lag natural frequencies can be observed compared to the skin thickness parameter. For the skin thickness parameter, both the stiffness and the mass are increased towards the parameter maximum. This effect decreases for the lower natural frequencies (F1, L1, F2) with increasing rotor speed and shows no change at nominal speed.

5.2.3 Frequency analysis – Spar Flange Thickness

For the spar flange thickness parameter, the parameter interval is divided asymmetrically in relation to the starting configuration, as can be seen Figure 9. The distance from the minimum to the starting configuration is much smaller than from the starting configuration to the maximum. The largest frequency variation, as can be seen in Figure 13, can be observed for this parameter for the lead-lag frequency (L2).

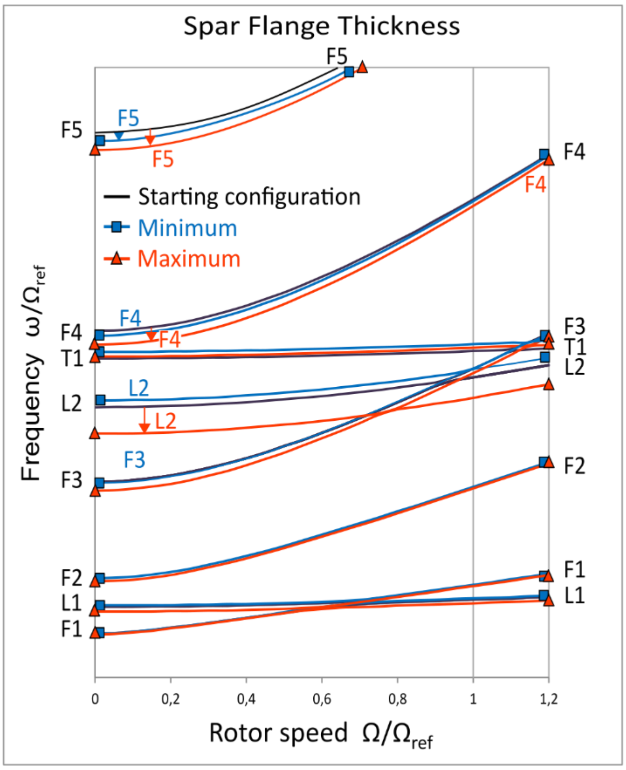

Figure 13: Frequency analysis – Spar Flange Thickness

Since, contrary to the parameter TCT the mass increases over the interval, the movement for the minimum and maximum of lead-lag frequencies of this parameter is exactly the opposite. The increase for lead-lag stiffness, which would lead to an increase in the natural frequency, is much smaller in contrast to the mass increase over the parameter interval. Together with the asymmetric distance from the start configuration to the parameter extrema, the lead-lag frequency is strongly decreased in the maximum and slightly increased in the minimum. Furthermore, even the first lead-lag mode (L1) is slightly reduced in the parameter maximum. For the flap frequencies (F3-F5), the magnitude is reduced both in the parameter minimum and in the maximum. In the starting configuration, however, the frequency is slightly higher than both parameter extrema. Looking at Figure 9 it can be seen that between the minimum and maximum the flap stiffness shows a stronger increase than the mass. The increase in flap stiffness decreases in the region of the extrema. In the region of the starting configuration, flap stiffness and mass assume a ratio that leads to an increase in the natural frequency in this region.

5.2.4 Frequency analysis – Distance Spar Center Main Radius

The maximum of the parameter DSCMR is similar to the parameter maximum of the SFT. For both parameter maxima, the mass is significantly increased in the airfoil interior. Accordingly, the upper flap frequencies (F3-F5) in relation to the start configuration are decreased. The frequency diagram is shown in Figure 14.

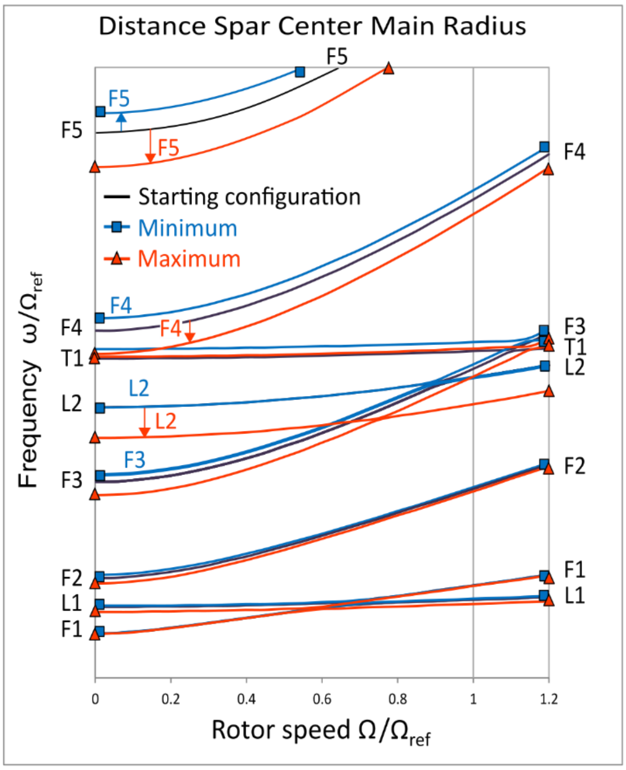

Figure 14: Frequency analysis – Distance Spar Center Main Radius

Since the parameter interval is unsymmetrically defined in relation to the starting configuration, the distances of the parameter minimum and maximum according to the starting configuration are different. With regard to the parameter maximum of the lead-lag frequencies (L1, L2), a similarity to the parameter SFT can be observed.

5.2.5 Frequency analysis – Distance Spar Trailing Edge

In opposite to the parameter SFT the parameter DFTE, as shown in Figure 8 and Figure 10, the structural properties in the parameter interval are much more varied due to the strong extension of the spar flanges in trailing edge direction. The effects of the extrema on the natural frequencies are shown in Figure 15.

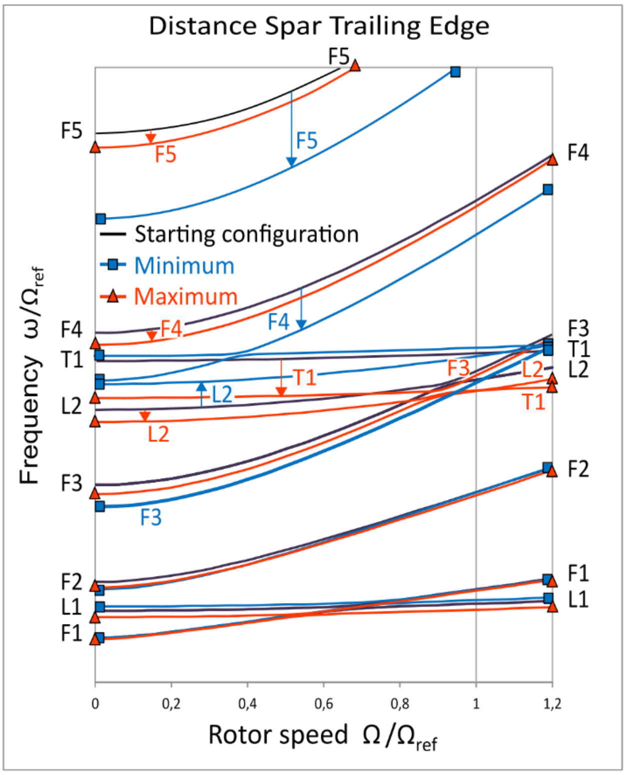

Figure 15: Frequency analysis – Distance Spar Trailing Edge

The flap frequencies (F3-F5) are reduced both in the parameter minimum and in the maximum compared to the starting configuration. In between the starting configuration and the parameter minimum, the mass decreases less than the flap stiffness. This strongly reduces the flap frequency in the parameter minimum. In the range of the starting configuration, the ratio of flap stiffness and mass results in an increased natural frequency compared to the parameter extrema. Since the mass increases strongly in the parameter maximum, the flap frequencies (F3-F5) are also reduced. It can be assumed that the flap frequencies (F3-F5) can be further increased in the range between the start configuration and the maximum, when the flap stiffness increases significantly more than the mass. For the lead-lag frequencies (L1, L2) only a decrease in between starting configuration and the parameter maximum is possible. In between the starting configuration and the parameter minimum the lead-lag stiffness, as can be seen in Figure 10, is less decreased than the mass. Therefore, lead-lag frequency increased in the parameter minimum. The strong increase of the mass over the parameter interval is also visible compared to the slight increase in torsion stiffness in the parameter maximum of the torsional frequency and is expressed in a reduction in this.

6. CONCLUSIONS

A process for generating and calculating the structural properties of rotor blade cross-sections was developed. In order to determine suitable design variables, a sensitivity as well as a frequency analysis were carried out by evaluating the structural properties and the natural frequencies as a result of different parameter variations. For the parameter variations, the following possibilities for structural adjustment could be identified:

1. The variation of the skin thickness mainly regulates torsional and lead-lag stiffness. A wide variation of the shear center and the center of gravity in the same orientation is created. Mainly torsional natural frequency and the second lead-lag natural frequency are influenced.
2. The stiffnesses are hardly affected by the implementation of the nose weight. Only the center of gravity is regulated by this parameter. The influence of the nose weight can be observed separately in the natural frequencies.
3. The reduced spar area due to the increase in nose weight may need to be compensated for by the spar parameters. The shear center is only slightly influenced by the parameter DTCTE.
4. The thickness of the spar flanges allows the tensile stiffness to be varied without any major influence on the axis positions.
5. The parameter DSCMR shows the influence of the spar web on the flap stiffness. This parameter has a strong influence on both lead-lag natural frequencies (L1, L2) at maximum.
6. The effective range for flap and lead-lag stiffness is set in the parameter interval for "Distance Spar Trailing Edge". For the flap natural frequency, the largest effective range occurs at the parameter center and decreases with proximity to the extrema. For lead-lag stiffness, the greatest increase is seen by extending the spar flanges to the trailing edge.

In the future, other cross-section topologies will be investigated with respect to its sensitivity to the resulting natural frequencies.

Author contact:

Franziska Becker franziska.becker@dlr.de

Steffen Kalow steffen.kalow@dlr.de

Rainer Bartels rainer.bartels@dlr.de

7. ACKNOWLEDGMENTS

The author acknowledges the work and ideas of colleagues from previous DLR-projects, like STAR, VicToria and Urban Rescue, which provided the basis for the presented paper.

REFERENCES

1. F. Becker, R. Bartels, S. Kalow und others, „Automatisierte Dimensionierung der inneren Struktur und der Eigenfrequenzen von Hubschrauberrotorblättern im Hinblick auf eine automatisierte Rotorblattoptimierung," *Deutscher Luft-und Raumfahrtkongress 2022,* 2022.

2. D. Desvigne, R. Coisnon, B. R. Michel, A. Thomas, J. P. Pinacho und E. Roca León, „Multi-Objective Industrial Optimization of High-Speed Helicopter Main Rotor Blades with Dynamically-Adapted Structural Properties," in *45th European Rotorcraft Forum*, 2019.

3. C. Stanger, M. Hollands, M. Keßler und E. Krämer, „Adaptation of the Dynamic Rotor Blade Modelling in CAMRAD for Fluid-Structure Coupling Within a Blade Design Process," in *New Results in Numerical and Experimental Fluid Mechanics IX*, Springer, 2014, p. 263–271.

4. J. C. Houbold und G. W. Brooks, „Differential Equations of Motion for Combined Flapwise Bending," *Chordwise Bending, and Torsion of Twisted Nonuniform Rotor Blades," NACA*

TN, Bd. 3905, 1957.

5. W. von Grünhagen, „Bestimmung der gekoppelten Schlagbiege-, Schwenkbiege- und Torsionsschwingungen für beliebige Rotorblätter mit Hilfe der Finite-Element-Methode (Computation of the coupled flap bending, lag bending and torsion oscillations for arbitrary rotor blades with the aid of the finite element method),“ *DFVLR IB,* p. 154–80, 1980.

6. H. Mainz, R. Bartels, B. van de Kamp, O. Schneider, G. Kuntze-Fechner und M. Hahn, „FTK ROTOR BLADES: DESIGN, MANUFACTURING AND TESTING,“ *43. European Rotorcraft Forum,* September 2017.

7. B. G. van der Wall, Grundlagen der Dynamik von Hubschrauber-Rotoren, Springer, 2018.

8. S. Kalow, B. van de Kamp, J. Riemenschneider, R. Bartels und H. Mainz, „Multidisciplinary Design Chain for model rotor blades,“ in *ICAS 2016*, 2016.

9. J. Bailly, B. Ortun und Y. Delrieux, „Recent advances in rotor aerodynamic optimization, including structural data update,“ *Journal of the American Helicopter Society,* Bd. 62, p. 1–11, 2017.

10. R. B. Haehnel, J. W. Lim, Y. Wenren, S. Tian und W. Yu, „Structural Analysis of a Rotorcraft Blade Design Using iVABS,“ *Vertical Flight Society's 79th Annual Forum &Technology Display, West Palm Beach, FL, USA,* 2023.

11. C. E. S. Cesnik und D. H. Hodges, „VABS: a new concept for composite rotor blade cross-sectional modeling,“ *Journal of the American helicopter society,* Bd. 42, p. 27–38, 1997.

12. B. van de Kamp und G. A. Wilke, „Automation of structural cross sectional rotor blade modelling for aeromechanical rotor blade optimization,“ 2018.